Geophysical Research Letters

RESEARCH LETTER
10.1002/2017GL076361

Understanding the Dynamics of Future Changes in Extreme Precipitation Intensity

Neil F. Tandon[1], **Xuebin Zhang**[1], **and Adam H. Sobel**[2,3]

[1]Climate Research Division, Environment and Climate Change Canada, Toronto, Ontario, Canada, [2]Department of Applied Physics and Applied Mathematics, Columbia University, New York, NY, USA, [3]Department of Earth and Environmental Sciences, Columbia University, New York, NY, USA

Key Points:
- Changes in the horizontal scale of ascending anomalies influence projected changes in subtropical extreme precipitation intensity
- These changes in horizontal scale are in turn associated with changes in vertical stability
- Near the equator, changes in the seasonal mean circulation may be an important factor influencing extreme precipitation intensity

Supporting Information:
- Supporting Information S1

Correspondence to:
N. F. Tandon,
neil.tandon@canada.ca

Citation:
Tandon, N. F., Zhang, X., & Sobel, A. H. (2018). Understanding the dynamics of future changes in extreme precipitation intensity. *Geophysical Research Letters*, *45*, 2870–2878. https://doi.org/10.1002/2017GL076361

Received 9 NOV 2017
Accepted 25 FEB 2018
Accepted article online 5 MAR 2018
Published online 30 MAR 2018

Abstract Climate model projections of extreme precipitation intensity depend heavily on the region: some regions will experience exceptionally strong increases in extreme precipitation intensity, while other regions will experience decreases in extreme precipitation intensity. These regional variations are closely related to regional changes in large-scale ascent during extreme precipitation events—that is, "extreme ascent"—but the drivers of extreme ascent changes remain poorly understood. Using output from a large ensemble of the Canadian Earth System Model version 2, we show that subtropical changes in extreme ascent likely result from changes in the horizontal scale of ascending anomalies, which are in turn associated with changes in vertical stability. Near the equator, changes in the seasonal mean circulation may be an important factor influencing extreme ascent, but this finding is model dependent.

Plain Language Summary We are all too familiar with the devastation that extreme precipitation events have caused in many regions, and there is a great need to understand how human activities are influencing such events. The large-scale upward velocity of air during an extreme precipitation event (i.e., "extreme ascent") plays a pivotal role in determining the amount of precipitation during the event (i.e., its "intensity"), but the mechanisms driving long-term changes in extreme ascent are poorly understood. Using simulations of climate change in a modern climate model, we show that, near the equator, changes in extreme ascent reflect a shift in the overall statistical distribution of vertical velocity. Elsewhere, however, the story is not so simple, and we show that another key factor influencing extreme ascent is the horizontal scale of the ascending motion. For example, long-term increases in horizontal scale lead to weaker extreme ascent and decreased extreme precipitation intensity in much of the subtropics, opposite to the increased extreme precipitation intensity that is expected over most of the globe. Thus, we explain long-term changes of extreme ascent in terms of well-established theories of atmospheric dynamics and improve our understanding of how these changes result from the long-term increase of surface temperature.

1. Introduction

Many countries are grappling with the impact of extreme precipitation. Heavy rainfall led to the Pakistan floods of 2010, which killed over 1,700 people and damaged or destroyed more than one million homes (Kirsch et al., 2012). Extreme precipitation led to the Alberta floods of 2013, which at the time was the costliest disaster in Canadian history (Milrad et al., 2015). There is great concern about how human activities are influencing the frequency and intensity of extreme precipitation events.

As Earth's global mean temperature increases, extreme precipitation events are expected to intensify over most of the globe (Kharin et al., 2013). This means that, for a given "return period," such as a once in 10-year or a once in 20-year event, the amount of precipitation associated with that event is expected to increase. Climate model simulations of future climate change project a widespread increase in maximum daily accumulated precipitation for return periods ranging from a year (Pfahl et al., 2017) to 20 years (Kharin et al., 2007, 2013). This widespread intensification of extreme precipitation is generally expected based on thermodynamic principles: as the atmosphere warms, saturation vapor pressure increases approximately following the Clausius-Clapeyron (CC) equation, which means that there is more moisture available in the atmosphere to condense into precipitation.

These projections, however, depend a lot on the region. Some regions are expected to experience exceptionally strong intensification of extreme precipitation (O'Gorman, 2012; Pfahl et al., 2017), while other regions are expected to experience decreases in extreme precipitation intensity (Pfahl et al., 2017). This regional variability is due to the effects of large-scale ascent during the extreme precipitation events, which we call "extreme ascent". In some regions, extreme ascent is expected to strengthen, favoring more precipitation, and in other regions, extreme ascent is expected to weaken, favoring less precipitation (Kang et al., 2013; Lu et al., 2014; O'Gorman & Schneider, 2009a; Pfahl et al., 2017). Extreme ascent changes are the greatest source of uncertainty in regional projections of extreme precipitation intensity (Pfahl et al., 2017), but the reasons for these changes remain poorly understood.

In this study, we examine the mechanisms driving changes in extreme ascent. For this, we use output from a 50-member ensemble of the Canadian Earth System Model version 2 (CanESM2) (Arora et al., 2011). Each member of this ensemble is run with the same prescribed "external forcings" (greenhouse gas concentration, aerosol concentration, etc.), and only the initial conditions of each ensemble member vary. Taking an average over such an ensemble greatly reduces any noise associated with internal climate variability and produces a clearer picture of the response to externally forced climate change (e.g., Deser et al., 2012). Furthermore, because we use only one model, intermodel differences do not confound the analysis, and we can develop a deeper understanding of the physical mechanisms at work in the model. This complements approaches in earlier studies that combine output from multiple models (Kharin et al., 2013; O'Gorman & Schneider, 2009b; Pfahl et al., 2017). We focus on changes of the 10-year maximum of daily precipitation between the 1981–2000 historical period and the 2081–2100 period when simulating a scenario of high greenhouse gas emissions. We refer to such long-term externally forced changes as "climatic changes." We will show that climatic changes in the horizontal scale of ascending anomalies are likely a key driver of climatic changes in extreme ascent.

2. Methods

CanESM2 is a fully coupled ocean-atmosphere climate model, with an approximate spatial resolution of 2.5° in the atmosphere (Arora et al., 2011). For all members of the CanESM2 ensemble, historical forcings were applied during 1950–2005, and thereafter, the forcings follow the high emission Representative Concentration Pathway 8.5 scenario (Taylor et al., 2012). Each run was branched in 1950 from one of five historical runs that were initialized in 1850. We confine our analysis to 20-year epochs in the past (1981–2000) and the future (2081–2100). Below we compare the CanESM2 results to results from a 40-member ensemble of the Community Earth System Model version 1 (CESM1) (Kay et al., 2015), which has approximately 1° spatial resolution in the atmosphere.

Composite means are computed from daily output, which is averaged over all ensemble members and over all days on which the 10-year maximum of daily accumulated precipitation occurs. Over a 20-year epoch and over a 50-member ensemble, such composite means are based on 100 samples at each model grid point. Fields calculated on days of extreme precipitation are generally indicated with a subscript "E," but when the field is computed at a representative pressure level (e.g., 500 hPa), the field is indicated with a lowercase subscript "e."

For short precipitation events that are poorly resolved by daily output (which is common in the subtropics), a reduction in the duration of the precipitation event also reduces the daily accumulated precipitation. Hence, changes in extreme precipitation intensity computed from daily output may result from changes in the subdaily time evolution of the precipitation event, rather than changes in the subdaily precipitation intensity. We take this into account when comparing our results to the results of earlier studies that examine extreme precipitation events using subdaily output (e.g., Nie & Sobel, 2016).

Seasonal mean vertical velocity is computed by taking the 3-month average of monthly mean vertical velocity centered around the month during which extreme precipitation typically occurs, m_E. We determine m_E by computing the mode of the month during which 10-year maximum precipitation occurs at each grid point after combining data from all realizations during the relevant epoch (see Figure S1b).

Climatic changes are computed by taking the epoch difference between 2081–2100 and 1981–2000. When normalizing with respect to temperature change, we use the zonal mean climatic change in annual mean surface air temperature at a given latitude (i.e., the zonal average of Figure S2a). We have also tested normalizing by the local change in near-surface air temperature on days of extreme precipitation (Figure S2b), and none of our key results was affected. We chose the normalization approach we did in order to strike a balance between the conventional approach of climate sensitivity studies, in which it is common to normalize

by global mean surface temperature change (e.g., Sherwood et al., 2015) and our desire to account for the meridional structure of temperature change.

Saturation vapor pressure is computed using equations (4.4.13) and (4.4.15) in Emanuel (1994), which closely approximate values in the Smithsonian Meteorological Tables. These are identical to the formulations used in CanESM2.

The horizontal scale of ascending anomalies, L_e, is determined at the center of a given grid point, (x, y), as follows:

1. On a given day of extreme precipitation, we compute the anomaly of daily mean vertical velocity at the relevant pressure level with respect to the monthly climatology during the relevant epoch.
2. We compute the zonal and meridional *e*-folding distance of this anomaly relative to (x, y), applying linear interpolation between grid point centers.
3. We divide the *e*-folding distances by $0.19 \times 2\pi$ to obtain the zonal and meridional scales of the corresponding waves, L_{ex} and L_{ey} respectively, expressed as inverse wavenumbers. As shown by Barnes and Hartmann (2012), this factor arises from the fact that the *e*-folding distance of a cosine wave is 0.19 times its wavelength.
4. We combine L_{ex} and L_{ey} using the Euclidean distance, $L_e = \sqrt{L_{ex}^2 + L_{ey}^2}$.
5. We average L_e over all days of extreme precipitation and over all realizations during the relevant epoch.

The historical values of L_e correspond well with eddy length scales computed using Fourier transforms (Barnes & Hartmann, 2012; Frierson et al., 2006; Kidston et al., 2010). For example, one can compare Figure S3a multiplied by 2π with Figure 1 of Kidston et al. (2010).

3. Extreme Precipitation Projections

Figure 1a shows the projected climatic change in extreme precipitation. We express this as a fractional change $\delta P_E / P_{E0}$ normalized by the zonal mean climatic change of annual mean surface temperature, where P_E is the composite mean of the 10-year maximum of daily precipitation and P_{E0} is P_E averaged over the historical period. (See section 2 for details.) Figure 1a shows that, over most of the globe, P_E is expected to increase. The light blue shading that dominates the picture coincides with the 6–7% K^{-1} increase that we expect from CC scaling. In much of the extratropics, the projected P_E increase is somewhat lower than CC scaling due to a reduction of the moist adiabatic lapse rate (O'Gorman & Schneider, 2009b).

In parts of the tropics, however, the projected increase is much greater than that expected from CC scaling. Furthermore, in much of the subtropics, P_E is expected to decrease. These large-scale patterns of $\delta P_E / P_{E0}$ qualitatively resemble the patterns computed from individual ensemble members (Figure S4), from other models, and for other return periods. (See Figures S5 and S6b; see also Kharin et al., 2013; Pfahl et al., 2017.) The large-scale patterns of $\delta P_E / P_{E0}$ differ substantially from patterns of annual mean precipitation change (Figure S6a), which is expected since the processes driving changes in mean and extreme precipitation are not necessarily the same.

The large deviations of $\delta P_E / P_{E0}$ from CC scaling are due to contributions from extreme ascent. As a starting point, we note that an extreme precipitation event is typically associated with strong vertical transport of moisture (O'Gorman & Schneider, 2009a). One can then determine the dynamical contribution to $\delta P_E / P_{E0}$ by isolating the portion of the vertical moisture transport that is associated with extreme ascent (see supporting information).

In agreement with Pfahl et al. (2017), Figure 1b shows that the dynamical part of $\delta P_E / P_{E0}$ explains much of the regional structure of $\delta P_E / P_{E0}$. For example, in the subtropical North Atlantic, the dynamical part of $\delta P_E / P_{E0}$ is approximately -15% K^{-1}, which explains most of the approximately -10% K^{-1} change in P_E in that region. (Thermodynamic effects cancel some of this dynamical effect; see Figure S7.) There are seven key regions where extreme ascent changes drive climatic decreases in P_E: the subtropical South Indian Ocean, the western equatorial Pacific, the subtropical North and South Pacific, northern South America, and the subtropical North and South Atlantic. These P_E decreases are especially noteworthy because they are opposite in sign to the P_E increase that is expected over most of the globe. As explained by O'Gorman (2015), dynamical contributions to $\delta P_E / P_{E0}$ are relatively weak in the extratropics, so hereafter, we confine our attention to the tropics and subtropics.

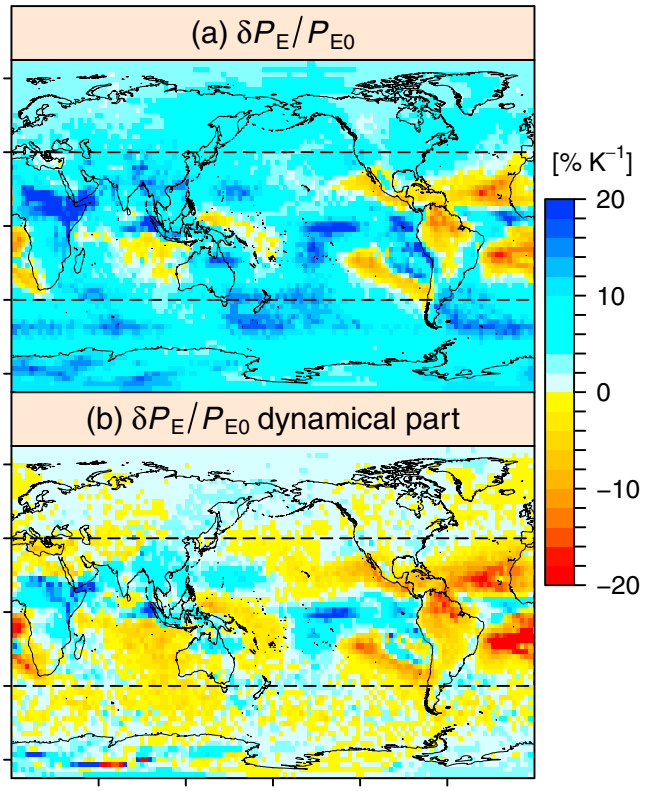

Figure 1. (a) The composite climatic fractional change in the 10-year maximum of daily precipitation. For this and all subsequent figures, computations are performed using output from the CanESM2 large ensemble, and climatic changes are normalized by the zonal mean change in annual mean surface temperature. (b) As in (a) for the dynamical part of extreme precipitation change. Dashed lines mark 40°S and 40°N, equatorward of which dynamical effects are especially important.

4. Role of Horizontal Scale of Ascent

To gain theoretical insight into the dynamical part of $\delta P_E/P_{E0}$, we model extreme ascent in the tropics and subtropics as

$$-\left[\frac{2H_p^2L_e^2}{(p_m-p_t)(p_s-p_m)}+\frac{N_e^2H_p^2}{f^2}\right]\omega_e=\frac{RH_p^2Q_e}{p_mf^2}, \tag{1}$$

where ω_e is the anomalous vertical pressure velocity (negative indicates ascent), L_e is the horizontal scale of ascending anomalies, Q_e is the diabatic heating anomaly, p_s and p_t are pressure at the surface and the tropopause, respectively, p_m is pressure at a representative level within the troposphere, H_p is the pressure depth of the troposphere, f is the Coriolis parameter, R is the gas constant for dry air, and N_e^2 is the dry stability. The latter is defined as

$$N_e^2=-\frac{RT_e}{p_m\theta_e}\frac{\partial\theta_e}{\partial p}, \tag{2}$$

where T_e is temperature and θ_e is potential temperature. The lowercase "e" subscripts indicate values on days of extreme precipitation evaluated at p_m. (This is distinct from the capital "E" subscript used above when the vertical level is not being specified.)

Equation (1) captures the effects of large-scale dynamical balance as well as convection (which influences diabatic heating). This formulation is based on the quasigeostrophic omega (QGω) equation, assuming that vertical velocity anomalies are wavelike in the horizontal and parabolic in the vertical. QGω-based formulations have been used in earlier studies of extreme precipitation (Nie & Sobel, 2016; Nie et al., 2016; O'Gorman, 2015), and we provide the derivation of our specific formulation in the supporting information.

We have found that tropopause pressure in the tropics and subtropics decreases by less than 3 hPa per degree of warming, in agreement with earlier studies of tropopause trends in models and reanalysis (Gettelman et al., 2009). Thus, we expect climatic changes in p_t and H_p to be a relatively minor contribution, and we treat them as constants in this study. In the supporting information, we perform scaling analysis showing that, in the tropics and subtropics, horizontal advection is likely a minor contribution to ω_e.

If $p_s \approx 1,000$ hPa and $p_t \approx 200$ hPa, and if we take $p_m = 500$ hPa, then $2H_p^2/[(p_m - p_t)(p_s - p_m)] \approx 9$. Furthermore, if L_e is comparable to the Rossby radius of deformation, $L_{Re} = N_e H_p/f$, then the term in (1) involving L_e^2 is about a factor of 9 larger than the term involving N_e^2. This is not strictly an order of magnitude difference, and L_e is substantially smaller than L_{Re} in much of the subtropics (see Figure S3), but it is nonetheless reasonable to consider a limit in which the term involving L_e^2 dominates over the term involving N_e^2. (We will verify below whether climatic changes of N_e^2 play a significant role.) In this limit, we can take the logarithm of (1) and impose a climate change perturbation to obtain

$$-\frac{\delta\omega_e}{\omega_{e0}} \approx \frac{\delta L_e^2}{L_{e0}^2} - \frac{\delta Q_e}{Q_{e0}}. \tag{3}$$

Near the equator, f vanishes, and (1) reduces to a form equivalent to the weak temperature gradient approximation (Bretherton & Sobel, 2003; Sobel et al., 2001). In this limit, the N_e^2 term dominates over the L_e^2 term in (1), and

$$-\frac{\delta\omega_e}{\omega_{e0}} \approx \frac{\delta N_e^2}{N_{e0}^2} - \frac{\delta Q_e}{Q_{e0}}. \tag{4}$$

Thus in the tropics and subtropics, we expect climatic changes in ω_e to be driven by some combination of changes in L_e, N_e^2 and Q_e.

Figure 2a shows $-\delta\omega_e/\omega_{e0}$ calculated at 500 hPa. This qualitatively resembles the dynamical part of $\delta P_E/P_{E0}$ (Figure 1b), which we expect since the latter is, by construction, driven entirely by changes in extreme ascent. (Here we focus on $-\delta\omega_e/\omega_{e0}$, since it is more analytically tractable than the dynamical part of $\delta P_E/P_{E0}$.) Climatic increases in L_e (Figure 2b) correspond closely with weaker extreme ascent ($-\delta\omega_e/\omega_{e0} > 0$), as we expect from (3).

Figure 2c shows $\delta N_e^2/N_{e0}^2$, and this is everywhere positive. This climatic N_e^2 increase is generally expected as the atmosphere warms, since the temperature lapse rate adjusts to remain close to moist adiabatic (e.g., Santer et al., 2005). While climatic increases in N_e^2 might contribute to decreases in extreme ascent in some regions (e.g., the subtropical North Atlantic), changes in N_e^2 do not explain the increases in extreme ascent elsewhere. Climatic changes in L_e appear to provide a stronger explanation for $-\delta\omega_e/\omega_e$ throughout the subtropics.

The fractional changes of L_e^2 are generally smaller in magnitude than $-\delta\omega_e/\omega_e$. Equation (3) suggests that any portion of $-\delta\omega_e/\omega_{e0}$ that is not explained by $\delta L_e^2/L_{e0}^2$ is likely explained by $\delta Q_e/Q_{e0}$. Nie and Sobel (2016) found that diabatic heating feeds back on large-scale ascent, and this feedback typically amplifies changes in large-scale ascent. Based on this, we expect that a climatic change of L_e^2 will produce a $-\delta\omega_e/\omega_{e0}$ response that is amplified compared to $\delta L_e^2/L_{e0}^2$.

Diabatic heating output is not available from the CanESM2 ensemble, but as detailed in the supporting information, one can estimate $\delta Q_e/Q_{e0}$ based on vertical moisture transport along a moist adiabat. As expected from Nie and Sobel (2016), Figure 2d shows that $\delta Q_e/Q_{e0}$ appears to amplify the change in extreme ascent associated with $\delta L_e^2/L_{e0}^2$. For example, in the subtropical North Atlantic, there is a climatic decrease in diabatic heating ($-\delta Q_e/Q_{e0} > 0$) that coincides with $\delta L_e^2/L_{w0}^2 > 0$ and $-\delta\omega_e/\omega_{e0} > 0$. As expected from (3), the combination $\delta L_e^2/L_{w0}^2 - \delta Q_e/Q_{e0}$ (Figure 2e) quantitatively accounts for most of $-\delta\omega_e/\omega_{e0}$. Inaccuracies in our estimate of diabatic heating and nonparabolic climatic changes in the vertical structure of ω_e might account for the remaining quantitative disagreement between Figures 2a and 2e. We have tested incorporating contributions from changes in horizontal advection, dry stability, and tropopause pressure, and these do not significantly improve the agreement.

Nie and Sobel (2016) came to similar findings regarding the role of the horizontal scale of ascent. They performed a series of experiments spanning a range of horizontal scales using a single column radiative-convective model coupled to a QGω-based parameterization of large-scale ascent. They found that,

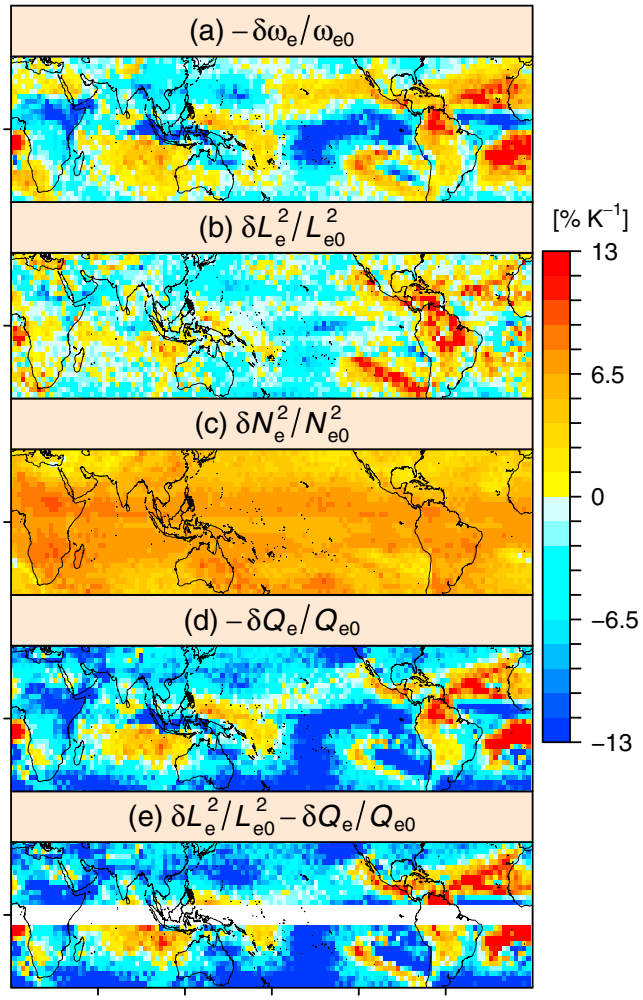

Figure 2. The composite climatic fractional changes of (a) extreme ascent at 500 hPa (positive changes indicate weakening extreme ascent), (b) square of the horizontal scale of ascending anomalies at 500 hPa, (c) dry stability averaged over 550 to 450 hPa, (d) the negative of the estimated diabatic heating at 500 hPa, and (e) the sum of the quantities in (b) and (d). As detailed in the text, we do not expect $\delta L_e^2/L_{e0}^2 - \delta Q_e/Q_{e0}$ to explain $-\delta\omega_e/\omega_{e0}$ near the equator, so panel (e) is masked equatorward of 5° latitude. Only latitudes between 40°S and 40°N are shown in each panel.

for a horizontal scale close to 1,000 km (corresponding approximately to the Rossby radius of deformation in the midlatitudes), large-scale ascent couples strongly to diabatic heating, and this generates large vertical velocity anomalies, which prolong the precipitation event. A longer precipitation event in the subtropics typically implies an increase of daily accumulated precipitation intensity (see section 2). Nie and Sobel (2016) found that a larger horizontal scale of ascent results in a shorter, less intense precipitation event.

Climatic changes in L_e also show close correspondence with $-\delta\omega_e/\omega_e$ near the equator. This is surprising because, as mentioned above, we do not expect L_e changes to play a significant role near the equator. In the equatorial Pacific, the climatic changes of ω_e coincide with changes in the large-scale seasonal mean vertical velocity, ω (Figure 3a). One might expect such a correspondence if a change in the seasonal mean circulation is associated with a shift of the overall statistical distribution of vertical velocity. The climatic increase in ω over the western equatorial Pacific is accompanied by a decrease over the eastern equatorial Pacific. These changes indicate a weakening of the Walker circulation, which is expected as the atmosphere warms and the dry stability increases (Held & Soden, 2006; Merlis & Schneider, 2011). These changes in the seasonal mean circulation may lead to L_e changes that partially compensate for the changes in vertical transport. That is, the climatic L_e changes near the equator might be a consequence of ω_e changes that are associated with changes

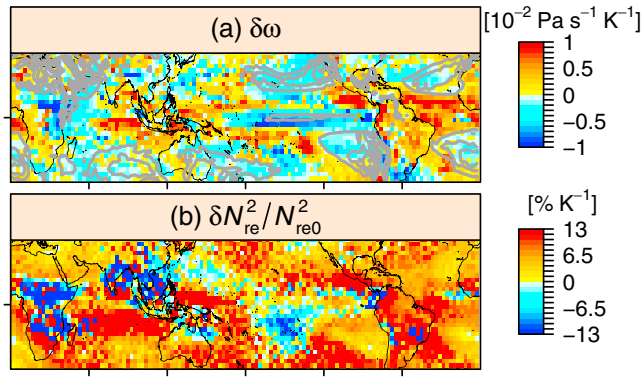

Figure 3. (a) The climatic change in seasonal mean vertical velocity at 500 hPa (shading) and the seasonal mean vertical velocity at 500 hPa during the historical period (gray contours). The contour interval is 0.015 Pa s^{-1}, with only positive (descending) values shown. (b) Composite climatic fractional change of effective stability, vertically averaged over 550 to 450 hPa. Only latitudes between 40°S and 40°N are shown.

in the seasonal mean circulation. More work is needed to confirm if this is the case and to establish more explicitly the physical links between the seasonal mean circulation and extreme ascent.

It is tempting to carry this logic further and explain subtropical climatic changes of extreme ascent in terms of changes in seasonal mean ascent. We consider this in more detail in the supporting information, along with the possible role of subgrid-scale convection changes. In particular, climatic changes in ω do not reliably explain changes in ω_e in the subtropics. Furthermore, near the equator, there appears to be model dependence as to whether the effects of seasonal mean circulation changes dominate over the effects of subgrid-scale convection changes.

5. Connection With Eddy Length Scale Theory

The previous section showed that subtropical climatic changes in extreme ascent likely result from changes in L_e. But what causes L_e to change in the subtropics? In these regions, one expects the horizontal scale of ascending anomalies to be influenced by the horizontal scale of eddies in the atmosphere. There have been various approaches to understanding the factors influencing eddy length scale. One common approach is to relate eddy length scale to the Rossby radius deformation, $L_{Re} = N_e H_p / f$. This leads to the expectation that eddy length scale increases as the dry stability increases (assuming, as argued above, that changes in tropopause pressure are a minor contribution). Since the dry stability climatically increases over most of the globe, this would imply that the eddy length scale should also increase over most of the globe. Such a global increase is indeed plausible when eddy length scale is computed from daily mean fields with no additional time filtering (Kidston et al., 2010). However, there is clearly not a global increase in L_e (Figure 2b).

One reason for this contrast is the effect of latent heat release. As saturated air rises, its moisture condenses and releases latent heat, which generates stronger ascent if the surrounding air is cooler. Thus, the stability experienced by rising saturated air is less than that experienced by dry air at the same temperature. We attempt to capture this by adopting an "effective stability,"

$$N_{re}^2 = \begin{cases} -\frac{RT_e}{p_m \theta_e} \frac{\partial \theta_e}{\partial p} & r_e < 98\% \\ -\frac{RT_e}{p_m \theta_e} \left[\frac{\partial \theta_e}{\partial p} - \left. \frac{\partial \theta_e}{\partial p} \right|_{\theta^*} \right] & r_e \geq 98\%, \end{cases} \tag{5}$$

where $\partial / \partial p|_{\theta^*}$ is the vertical derivative along a moist adiabat and r_e is relative humidity (RH) on the climate model grid evaluated at p_m on days of extreme precipitation. When grid-scale RH is sufficiently subsaturated, the effective stability equals the dry stability, and when grid-scale RH is nearly saturated, it incorporates a term accounting for latent heat release. This closely resembles the effective stability formulation of O'Gorman (2011), except that we give additional consideration to the role of RH (Booth et al., 2015). We provide additional discussion of this formulation and its derivation in the supporting information.

Compared to the climatic changes of dry stability (Figure 2c), the climatic changes of N_{re}^2 (Figure 3b) show closer correspondence to the changes in L_e. Notably, N_{re}^2 does not increase everywhere, and it shows decreases

in some regions (e.g., the subtropical South Pacific) where there are also L_e decreases. Climatic changes in N_{re}^2 do not explain changes in L_e in the eastern equatorial Pacific, and we do not expect them to: as discussed above, L_e changes here may be a consequence rather than a cause of ω_e changes that are linked to changes in the seasonal mean circulation.

Additional analysis reveals that climatic changes in r_e are crucial for producing decreases in N_{re}^2. We confirmed this by computing changes in N_{re}^2 holding r_e fixed at its historical value. This makes it difficult to pinpoint the precise cause of the climatic increase in extreme ascent in parts of the subtropics. The causality can go both ways: stronger extreme ascent (due perhaps to an increase of seasonal mean ascent or stronger subgrid-scale convection) can produce an increase in r_e and a decrease in N_{re}^2; conversely, an increase in r_e can produce a decrease in N_{re}^2, which produces stronger extreme ascent. More work is needed to understand the precise chain of causality in regions where there is climatic strengthening of extreme ascent.

In much of the subtropics, however, climatic changes in N_{re}^2 reflect increases in dry stability, and thus, the chain of causality appears to be more straightforward: a climatic increase in stability leads to an increase in the horizontal scale of ascending anomalies, which leads to weaker extreme ascent. Thus, in the subtropics, we have established a key physical mechanism linking long-term warming with climatic decreases of extreme precipitation intensity.

6. Concluding Remarks

In agreement with Pfahl et al. (2017), we have found that regional patterns of extreme precipitation projections are strongly influenced by climatic changes in extreme ascent (ω_e). We have shown that climatic ω_e changes in the subtropics likely result from changes in the horizontal scale of ascent (L_e), which are in turn associated with changes in effective stability (N_{re}^2). In regions where extreme precipitation intensity is projected to decrease, an especially clear chain of causality emerges: an increase in N_{re}^2 (reflecting the expected increase of dry stability with warming) leads to an increase in L_e, which in turn leads to weaker extreme ascent. In other parts of the subtropics, climatic L_e decreases coincide with N_{re}^2 decreases, but clarifying the ultimate cause of the N_{re}^2 decreases requires more work.

Near the equator, climatic changes in ω_e appear to be associated with changes in the seasonal mean circulation, such as the weakening Walker circulation. This result, however, is model dependent. Overall, our results help to link climatic changes of extreme ascent with other physical processes that are well-established consequences of a warming atmosphere.

One limitation of our study is that it relies entirely on climate model output to investigate the mechanisms responsible for extreme precipitation change. The climatology of annual maximum precipitation in CanESM2 resembles the climatology of annual maximum precipitation in observations and other climate models (Pfahl et al., 2017). This gives us some confidence that the physical processes driving climatic changes of 10-year maximum precipitation in CanESM2 are reflective of physical processes at work in the real world. Direct physical attribution of observed climatic changes in extreme precipitation intensity may be feasible in the extratropics because these changes are expected to be primarily thermodynamic (Westra et al., 2013), although over the short observational record, internal climate variability can be a significant confounding factor (Hoerling et al., 2016; Xue et al., 2017).

Physical attribution of extreme precipitation changes is more challenging in the tropics and subtropics because of the role of large-scale vertical motions, for which very few direct observations exist. The reliability of reanalysis products in the tropics and subtropics may be questionable because of the sparse observations available for constraining the dynamics of the underlying model. We are currently exploring the suitability of various reanalyses and station-based measurements for physically attributing observed changes in extreme precipitation. Continued and improved observational monitoring will greatly facilitate future investigations of the physical mechanisms driving extreme precipitation change.

Acknowledgments
We thank Ji Nie and Martin Singh for helpful discussions, Michael Sigmond and John Fyfe for valuable feedback on the draft manuscript, and Stephan Pfahl and an anonymous reviewer for constructive comments on the submitted manuscript. We acknowledge Environment and Climate Change Canada's Canadian Centre for Climate Modelling and Analysis for executing and making available the CanESM2 large ensemble simulations used in this study and the Canadian Sea Ice and Snow Evolution (CanSISE) Network for proposing the simulations. All data used in this study are publicly available. Output from the CanESM2 large ensemble may be found at http://collaboration.cmc.ec.gc.ca/cmc/cccma/CanSISE/output/CCCma/CanESM2/. All other data used in this study have been cited, with details provided in the list of references.

References

Arora, V. K., Scinocca, J. F., Boer, G. J., Christian, J. R., Denman, K. L., Flato, G. M., et al. (2011). Carbon emission limits required to satisfy future representative concentration pathways of greenhouse gases. *Geophysical Research Letters*, *38*, L05805. https://doi.org/10.1029/2010GL046270

Barnes, E. A., & Hartmann, D. L. (2012). The global distribution of atmospheric eddy length scales. *Journal of Climate*, *25*, 3409–3416. https://doi.org/10.1175/JCLI-D-11-00331.1

Booth, J. F., Polvani, L., O'Gorman, P. A., & Wang, S. (2015). Effective stability in a moist baroclinic wave. *Atmospheric Science Letters*, *16*, 56–62. https://doi.org/10.1002/asl2.520

Bretherton, C. S., & Sobel, A. H. (2003). The Gill model and the weak temperature gradient approximation. *Journal of the Atmospheric Sciences*, *60*, 451–460. https://doi.org/10.1175/1520-0469(2003)060<0451:TGMATW>2.0.CO;2

Deser, C., Phillips, A., Bourdette, V., & Teng, H. (2012). Uncertainty in climate change projections: The role of internal variability. *Climate Dynamics*, *38*, 527–546. https://doi.org/10.1007/s00382-010-0977-x

Emanuel, K. A. (1994). *Atmospheric convection* (580 pp.). New York: Oxford University Press.

Frierson, D. M. W., Held, I. M., & Zurita-Gotor, P. (2006). A gray-radiation aquaplanet moist GCM. Part I: Static stability and eddy scale. *Journal of the Atmospheric Sciences*, *63*, 2548–2566. https://doi.org/10.1175/JAS3753.1

Gettelman, A., Birner, T., Eyring, V., Akiyoshi, H., Bekki, S., Brühl, C., et al. (2009). The tropical tropopause layer 1960–2100. *Atmospheric Chemistry and Physics*, *9*, 1621–1637. https://doi.org/10.5194/acp-9-1621-2009

Held, I. M., & Soden, B. J. (2006). Robust responses of the hydrological cycle to global warming. *Journal of Climate*, *19*, 5686–5699. https://doi.org/10.1175/JCLI3990.1

Hoerling, M., Eischeid, J., Perlwitz, J., Quan, X.-W., Wolter, K., & Cheng, L. (2016). Characterizing recent trends in U.S. heavy precipitation. *Journal of Climate*, *29*, 2313–2332. https://doi.org/10.1175/JCLI-D-15-0441.1

Kang, S. M., Polvani, L. M., Fyfe, J. C., Son, S.-W., Sigmond, M., & Correa, G. J. P. (2013). Modeling evidence that ozone depletion has impacted extreme precipitation in the austral summer. *Geophysical Research Letters*, *40*, 4054–4059. https://doi.org/10.1002/grl.50769

Kay, J. E., Deser, C., Phillips, A., Mai, A., Hannay, C., Strand, G., et al. (2015). The Community Earth System Model (CESM) large ensemble project: A community resource for studying climate change in the presence of internal climate variability. *Bulletin of the American Meteorological Society*, *96*, 1333–1349. https://doi.org/10.1175/BAMS-D-13-00255.1

Kharin, V. V., Zwiers, F. W., Zhang, X., & Hegerl, G. C. (2007). Changes in temperature and precipitation extremes in the IPCC ensemble of global coupled model simulations. *Journal of Climate*, *20*, 1419–1444. https://doi.org/10.1175/JCLI4066.1

Kharin, V. V., Zwiers, F. W., Zhang, X., & Wehner, M. (2013). Changes in temperature and precipitation extremes in the CMIP5 ensemble. *Climatic Change*, *119*, 345–357. https://doi.org/10.1007/s10584-013-0705-8

Kidston, J., Dean, S. M., Renwick, J. A., & Vallis, G. K. (2010). A robust increase in the eddy length scale in the simulation of future climates. *Geophysical Research Letters*, *37*, L03806. https://doi.org/10.1029/2009GL041615

Kirsch, T. D., Wadhwani, C., Sauer, L., Doocy, S., & Catlett, C. (2012). Impact of the 2010 Pakistan floods on rural and urban populations at six months. *PLOS Currents*, *4*, e4fdfb212d2432. https://doi.org/10.1371/4fdfb212d2432

Lu, J., Ruby Leung, L., Yang, Q., Chen, G., Collins, W. D., Li, F., et al. (2014). The robust dynamical contribution to precipitation extremes in idealized warming simulations across model resolutions. *Geophysical Research Letters*, *41*, 2971–2978. https://doi.org/10.1002/2014GL059532

Merlis, T. M., & Schneider, T. (2011). Changes in zonal surface temperature gradients and Walker circulations in a wide range of climates. *Journal of Climate*, *24*, 4757–4768. https://doi.org/10.1175/2011JCLI4042.1

Milrad, S. M., Gyakum, J. R., & Atallah, E. H. (2015). A meteorological analysis of the 2013 Alberta flood: Antecedent large-scale flow pattern and synoptic-dynamic characteristics. *Monthly Weather Review*, *143*, 2817–2841. https://doi.org/10.1175/MWR-D-14-00236.1

Nie, J., & Sobel, A. H. (2016). Modeling the interaction between quasigeostrophic vertical motion and convection in a single column. *Journal of the Atmospheric Sciences*, *73*, 1101–1117. https://doi.org/10.1175/JAS-D-15-0205.1

Nie, J., Shaevitz, D. A., & Sobel, A. H. (2016). Forcings and feedbacks on convection in the 2010 Pakistan flood: Modeling extreme precipitation with interactive large-scale ascent. *Journal of Advances in Modeling Earth Systems*, *8*, 1055–1072. https://doi.org/10.1002/2016MS000663

O'Gorman, P. A. (2011). The effective static stability experienced by eddies in a moist atmosphere. *Journal of the Atmospheric Sciences*, *68*, 75–90. https://doi.org/10.1175/2010JAS3537.1

O'Gorman, P. A. (2012). Sensitivity of tropical precipitation extremes to climate change. *Nature Geoscience*, *5*, 697–700. https://doi.org/10.1038/ngeo1568

O'Gorman, P. A. (2015). Precipitation extremes under climate change. *Current Climate Change Reports*, *1*, 49–59. https://doi.org/10.1007/s40641-015-0009-3

O'Gorman, P. A., & Schneider, T. (2009a). Scaling of precipitation extremes over a wide range of climates simulated with an idealized GCM. *Journal of Climate*, *22*, 5676–5685. https://doi.org/10.1175/2009JCLI2701.1

O'Gorman, P. A., & Schneider, T. (2009b). The physical basis for increases in precipitation extremes in simulations of 21st-century climate change. *Proceedings of the National Academy of Sciences of the United States of America*, *106*, 14,773–14,777. https://doi.org/10.1073/pnas.0907610106

Pfahl, S., O'Gorman, P. A., & Fischer, E. M. (2017). Understanding the regional pattern of projected future changes in extreme precipitation. *Nature Climate Change*, *7*, 423–427. https://doi.org/10.1038/nclimate3287

Santer, B. D., Wigley, T. M. L., Mears, C., Wentz, F. J., Klein, S. A., Seidel, D. J., et al. (2005). Amplification of surface temperature trends and variability in the tropical atmosphere. *Science*, *309*, 1551–1556. https://doi.org/10.1126/science.1114867

Sherwood, S. C., Bony, S., Boucher, O., Bretherton, C., Forster, P. M., Gregory, J. M., & Stevens, B. (2015). Adjustments in the forcing-feedback framework for understanding climate change. *Bulletin of the American Meteorological Society*, *96*, 217–228. https://doi.org/10.1175/BAMS-D-13-00167.1

Sobel, A. H., Nilsson, J., & Polvani, L. M. (2001). The weak temperature gradient approximation and balanced tropical moisture waves. *Journal of the Atmospheric Sciences*, *58*, 3650–3665. https://doi.org/10.1175/1520-0469(2001)058<3650:TWTGAA>2.0.CO;2

Taylor, K. E., Stouffer, R. J., & Meehl, G. A. (2012). An overview of CMIP5 and the experiment design. *Bulletin of the American Meteorological Society*, *93*, 485–498. https://doi.org/10.1175/BAMS-D-11-00094.1

Westra, S., Alexander, L. V., & Zwiers, F. W. (2013). Global increasing trends in annual maximum daily precipitation. *Journal of Climate*, *26*, 3904–3918. https://doi.org/10.1175/JCLI-D-12-00502.1

Xue, T., Tang, G., Sun, L., Wu, Y., Liu, Y., & Dou, Y. (2017). Long-term trends in precipitation and precipitation extremes and underlying mechanisms in the U.S. Great Basin during 1951–2013. *Journal of Geophysical Research: Atmospheres*, *122*, 6152–6169. https://doi.org/10.1002/2017JD026682